Chapter 5

Conclusions

This chapter makes a final review of the results achieved in our research. First, we briefly report chronologically the steps of the investigations, and then we highlight the contributions this thesis has brought to the field of medical image registration. Finally, some remarks for future work are given.

When I started working on this thesis, algorithms based on mutual information had recently appeared in literature, with impressing results: they could be applied to a wide range of images, and the accuracy was excellent.

The initial motivation of my work was as a natural extension of the research of a colleague, who devised an operator to extract the skull in CT and MR images. My goal was to employ these landmarks for the purpose of registration. Compared to the mutual information algorithms, ours seemed slow, too much memory consuming and tailored to a single application. Indeed, extracting the skull demanded high CPU power, and then sometimes he alignment process would get trapped into a local maximum after many hours of computation.

Little by little, as I gained knowledge in the field results improved. Firstly, the segmentation became faster and more reliable, thanks to the dedication of A. López. Afterwards, improvements in the hierarchical structure and the alignment function led to a shortening of two orders of magnitude in the final computation time, with more satisfactory convergence properties.

Then we engaged on a project for an external evaluation of the accuracy of the algorithm with a large database of images, to be held at Vanderbilt University. This motivated several improvements, to deal with different field of view in the images, and also some observations for a particular MR setting, where the creaseness could not segment the skull so well.

Finally, we designed an experiment to test the robustness of the algorithm, which consisted on recovering hundreds of known misregistrations of the registered images. The same procedure was run on a mutual information algorithm, and statistics were compared.

Chapter 2 gives full report of these experiments. The hierarchical structure permitted a fast and more robust convergence, since a large number of seeds could be

tested at coarser levels. Also, the initial exhaustive search could provide a set of seeds which would converge to a proper value. For a few cases where this scheme failed, we added a fast rough alignment based on the detection of the principal axis of the skull in the image.

The external evaluation confirmed our visual assessments. All registrations had succeeded, and the accuracy achieved was comparable to the pixel size of the images. Our method ranked the first for an MR modality where the skull could be segmented particularly, and it ranked amongst those based on mutual information for other MR modalities. Also, the robustness experiments showed similar number for creaseness-based and MI -based methods.

After publish a paper with these results, we wondered whether the same algorithm would success on other image modalities depicting creases. We mainly found two examples in literature: vessels and the convolutions of the brain.

Vessels are visible on most modalities, but we focused on retinographies because the methods published so far, being highly heuristic al and poorly validated, clearly left room for improvement.

We adapted the algorithm to work with 2D images, and run it with a set of a about one hundred pairs of images. To our surprise, it easily succeeded for all. We decided to test it further, for fist time in literature, for the purpose of to align long sequences of *SLO* video images. The research was specially motivating because the hospital providing the sequences would actually use the algorithm for diagnosis. Therefore we studied the robustness and accuracy for different sequences and parameters, and concluded that our algorithm was perfectly suitable. Also, with the collaboration of one member of the team in the hospital, we produced a first prototype with the requirements needed for diagnosis, e.g. to depict the contents of a particular landmark in the vessel tree through the sequence.

Another interesting result was an enhancement of the algorithm in order to model, by means of local transformations, the elastic deformations in the image produced by the optics of the eye. Chapter 3 reports the details of the registration of 2D retinographies.

The third application of the algorithm, explained in chapter 4 was in the field of intraoperative ecographic images, which was started after the collaboration of the CISG group in London and Dr. Molet, at the Hospital de Sant Pau. Speaking in general, the goal is to measure the shift of the brain which occurs after the craniotomy. Many other groups are working intensively in the field, but our primary interest was to investigate the use of creases to register the ecographic images in the operating room to pre-operative images of the same patient.

However, before this could be done, we needed to build a system able to track the position of the transducer and grab the video images on real time. Another important issue was to calibrate the probe in the external coordinate system.

We spend some time on this matter, and finally we achieved an error comparable to that of the tracking system. Then, the next step was to test it in a real environment, but because real surgery was not available to us at that moment, we run the system on a phantom, an in-vitro human brain of an adult.

This permitted a number of interesting experiments, unfeasible for the case of a patient. We could, for instance, scan the whole brain to produce a volume image,

and then register the image to an MR image of the same brain. We employed for this purpose our algorithm, and the visual inspection of matching proved very accurate. To our notice, this is the first ultrasound to MR registration in literature.

A handy way to visualise the registration was to depict for each video frame the corresponding cutout in the MR image. Some frames showed some sort of misregistration, produced by the errors in the coordinates given by the tracker. The obvious solution was to produce another version of the registration algorithm, this time to register 2D ecographies to 3D MR volumes. This choice was very suitable given the features of the ecographic images: the creaseness operator extracted the sulci with reasonable confidence, and the algorithm was able to discard artifacts and non-matching surfaces. We visually inspected the results, and found them very satisfactory given the accuracy depicted by the MR images.

In sum the main contributions of this dissertations are:

- CT to MR volume registration:
  - we have proposed a new retrospective algorithm which takes the skull as the rigid landmark reference and employs a hierarchical approach. The method takes less than 4 minutes to complete on images of size about $250 \times 250 \times 100$ pixels.
  - The method is robust against large misregistrations with a mean error of 0.6 to 1.9 mm, for some cases lower than the that of mutual information (1.7 to 6.2 mm).
  - The validation, covering a large database of images and carried out externally within the Vanderbilt project, has achieved consistent rms errors (rank out of a group of 16 in brackets): 1.7 mm for CT –MR–PD (7), 3.4 mm for CT-MR–T1 (8) and 1.6 mm CT-MR–t2 (1).
- In the field of retinographies:
  - The 2–D version of the previous algorithm is successful at registering pairs of different modalities and taken with some time interval. Experiments include cases considered as difficult in published papers.
  - Studies have covered, for the first time, long sequences of *SLO* video frames. Despite their variability and wide range of misregistrations, the visual inspection of the results for three series comprising about 1000 of frames each has given success rates higher than 80%.
  - The algorithm has been tuned in speed and robustness for a real clinical application, currently running in a hospital. Initial validations have shown figures similar to those obtained manually.
  - The non-rigid transformations caused by the optics of the eye have been modelled by an extension of the algorithm which works in a local fashion.
- For intraoperative volume *us* –MR registration:
  - We have built a prototype software to acquire and compound ecographies, which includes a comparison of three different phantoms for calibration.

The final rms error achieved, about 4 mm, is reasonable considering the accuracy of the magnetic tracker.

- We have registered successfully, for first time in literature, the compounded volume ecography to an MR image of a human brain, by means of our creaseness-based algorithm. The visual inspection of pairs of each pairs of corresponding images, this is, the B-scan together with the corresponding cutout, has revealed a very good alignment.
- We have proposed a new 2D–3D creaseness-based registration algorithm, and tested it on two pairs of modalities: B-scan to ecography volume and B-scan to MR volume. We have validated manually each the sequences of images for each case, and results show that the process improves the alignment in $70-90$ % of frames for the first pair, and 50 % for the second. The method proposed is, again, a novelty in literature, and potentially will permit to measure the deformation of the brain during surgery, as well as to provide the landmarks to update the MR volume by means of an elastic deformation.

We would like to finish with a few remarks directed to possible future work. As we stated in the introduction, we thought it was only fair to try to revert the results of the investigation into the society, which meant to translate the implementation of the algorithms for real clinical practise. Many hours of work have been devoted to this purpose, but still we feel that very little has actually come out, the retinographies being the only success. As for the case of neurosurgery, we found difficulties impossible to overcome, even with the best help of the physicians. For instance, things such as transferring images was at that time a lengthy task and matter of random because the devices and the network were poorly set.

Still, initially we managed to design and validate an application for stereotactic surgery, which could detect the artificial landmarks in the stack of images and calibrate the coordinate systems. Our plan was to further extend this program to include also the in-theatre ecographic image but this did not happen to be possible at that time.

However, recently the collaborating hospital has renewed all the equipment, and therefore the primary goal becomes again feasible. Perhaps with the results presented here, the work left now as future will some day be put into practise.

Bellaterra, November 2001

Glossary of terms

B-scan Every single frame of a ecography video sequence. (135)

$\mathcal{C}$ Image in cuberille in the coordinates of $\mathcal{B}$. (172)

C.N. Condition number of a convergence experiment (232)

CSLO Confocal Scanning laser opthalmoscope (76)

D Dynamic image: for the registration algorithm, the image which iteratively transformed during the optimization. (39)

ftol Tolerance required to the Simplex algorithm to converge (91)

GM Global Multiple seed search (107)

GS Global Single seed search (107)

LSEC Level-Set Extrinsic Curvature (35)

MD Mean distance between two transformations (59)

mi Mutual information (61)

NC Normalized correlation (95)

NC Normalized matching (96)

ROI Region of interest of an image

S Static image: for the registration algorithm, the image which is not transformed during the optimization. (39)

SLO Scanning laser opthalmoscope (76)

TRE Target Registration Error (67)

US Ultrasound or ecographic image

$\mathcal{B}$ Ecographic image. (172)

VOI Volume Of Interest (67)

Appendix A

Specifications of the transformations

Many valid definitions of transformation matrices exist, each employing different notation and models. In the following pages we specify for completeness the transformation models employed throughout the thesis.

Given the coordinates of a pixel in the output image, $O_{x,y,z}$ and in the input image, $I_{x,y,z}$, and the transformation matrix M, they are related by the following equation:

$$O = I * M \tag{A.1}$$

We define the following transformation primitives:

$$Rot(x,y,z) := \begin{pmatrix} C_yC_z & C_z * S_x * S_y - C_x * S_z & C_x * C_z * S_y + S_x * S_z & 0 \\ C_y * S_z & C_x * C_z + S_x * S_y * S_z & -C_z * S_x + C_x * S_y * S_z & 0 \\ -S_y & C_y * S_x & C_x * C_y & 0 \\ 0 & 0 & 0 & 1 \end{pmatrix} \tag{A.2}$$

with $C_x = \cos x, S_x = \sin x$ etc.

$$Tras(x,y,z) := \begin{pmatrix} 1 & 0 & 0 & 0 \\ 0 & 1 & 0 & 0 \\ 0 & 0 & 1 & 0 \\ -x & -y & -z & 1 \end{pmatrix} \tag{A.3}$$

$$Sca(x,y,z) := \begin{pmatrix} x & 0 & 0 & 0 \\ 0 & y & 0 & 0 \\ 0 & 0 & z & 0 \\ 0 & 0 & 0 & 1 \end{pmatrix} \tag{A.4}$$

Given an image of m columns and n rows, we define translation from the origin to the centre, and viceversa:

$$M_{oc}(m,n) := Tras(-m,-n,0) \tag{A.5}$$

$$M_{co}(m,n) := Tras(m,n,0) \tag{A.6}$$

In terms of these primitives we define more complex transformations:

Rigid

$$M_R(T_x, T_y, \phi_z) := \qquad Tras(-T_x, -T_y, 0) M_{oc} Rot(0, 0, \phi_z) M_{co} \tag{A.7}$$

Scaled centred

$$M_R(T_x, T_y, \phi_z, S_x, S_y) := Tras(-T_x, -T_y, 0) M_{oc} Rot(0, 0, \phi_z) Sca(S_x, S_y, 0) M_{co} \tag{A.8}$$

Scaled non centred

$$M_R(T_x, T_y, \phi_z, S_x, S_y) := Tras(-T_x, -T_y, 0) M_{oc} Rot(0, 0, \phi_z) M_{co} Sca(S_x, S_y, 0) \tag{A.9}$$

Appendix B

Graphical results for the Vanderbilt database.

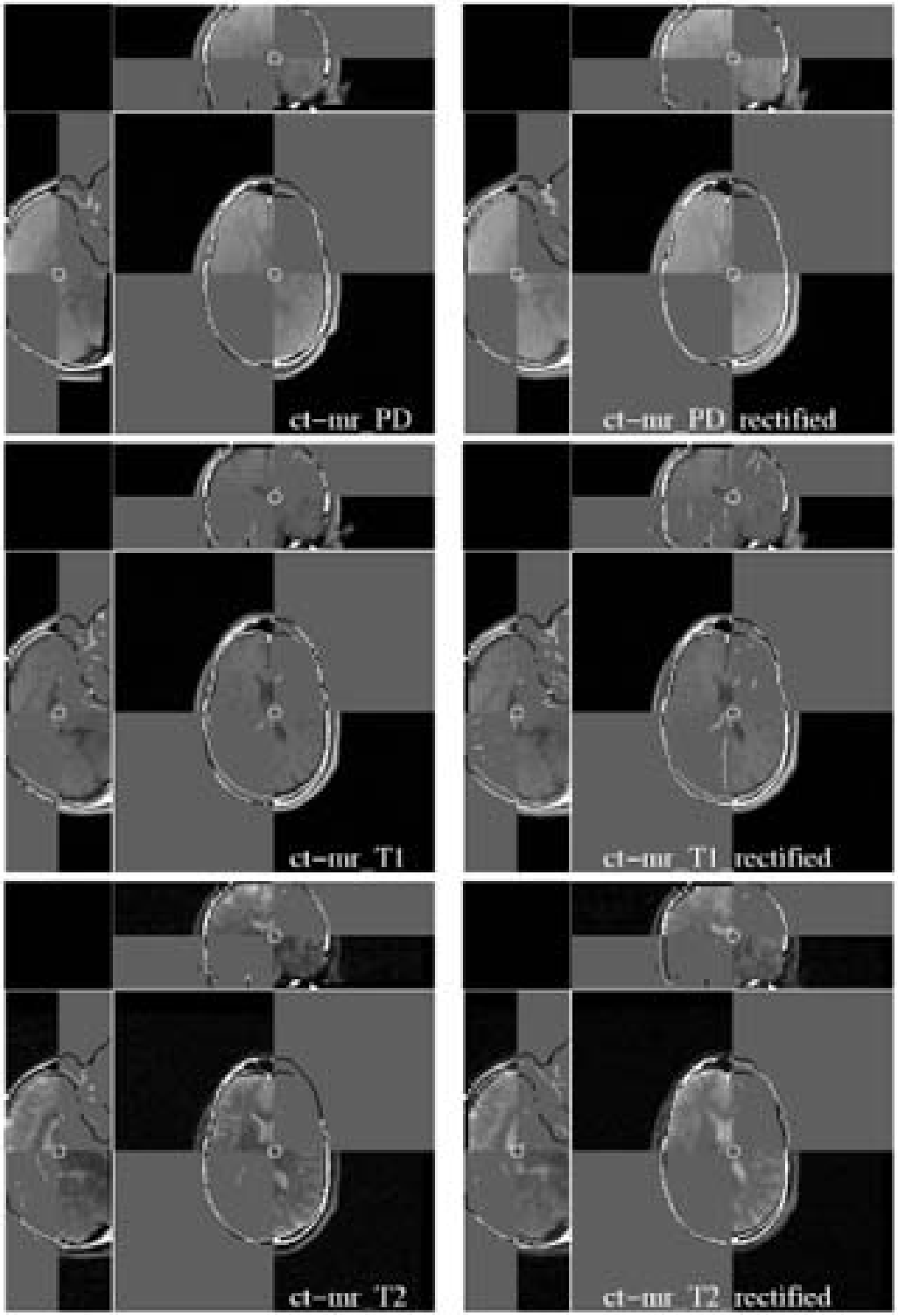

Figure B.1: Visual registration for patient 1

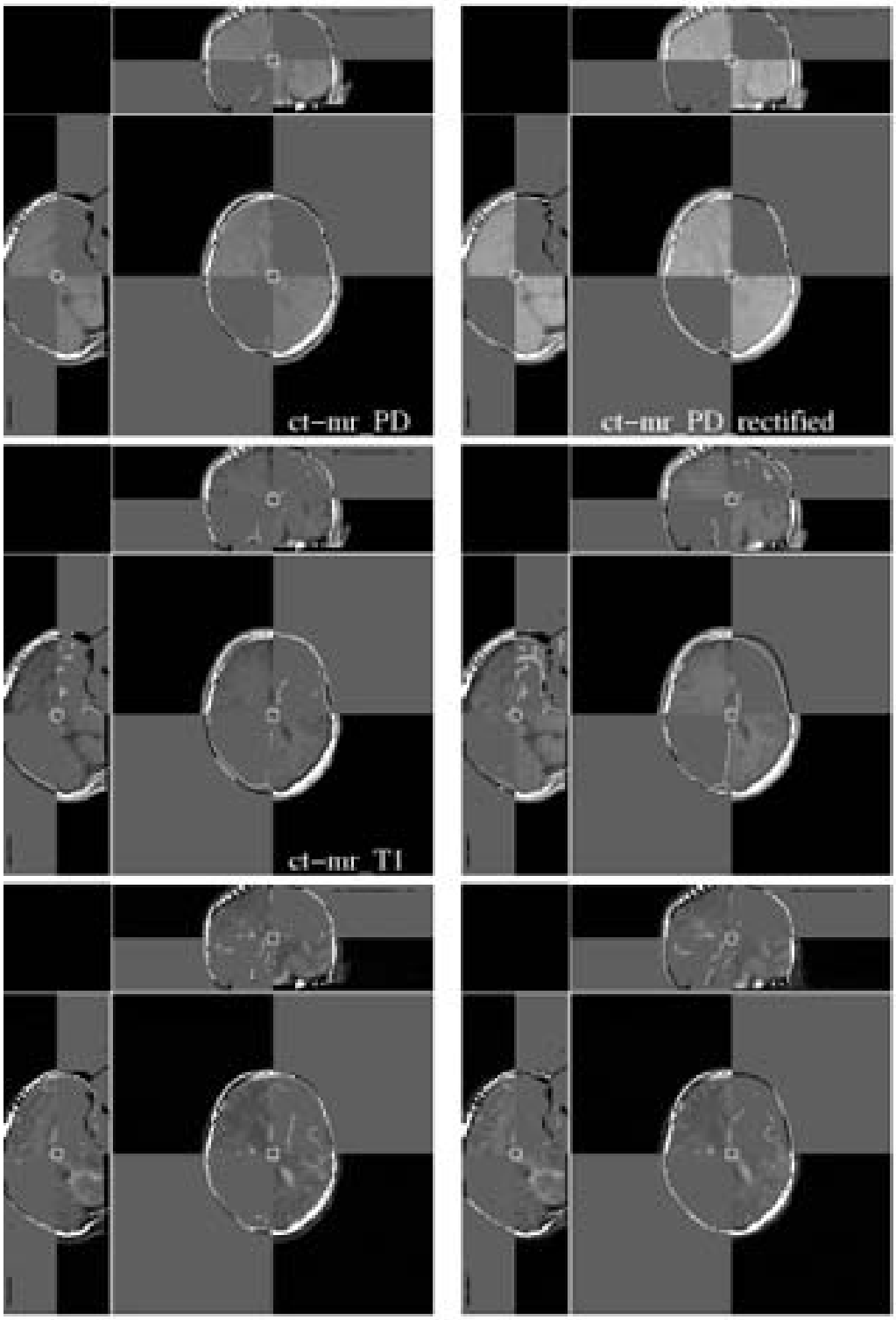

Figure B.2: Visual registration for patient 7–A

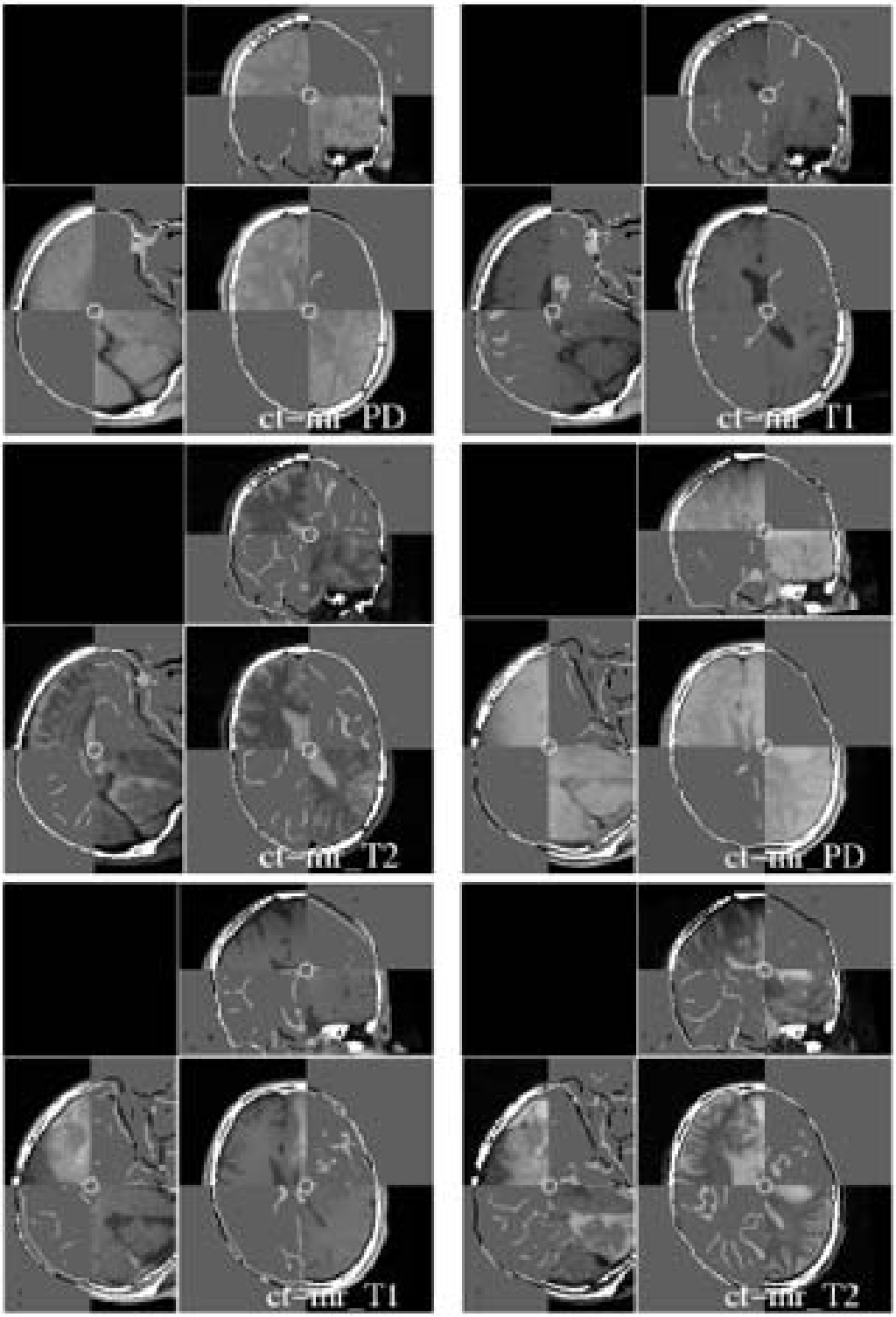

Figure B.3: Visual registration for patient 2–B

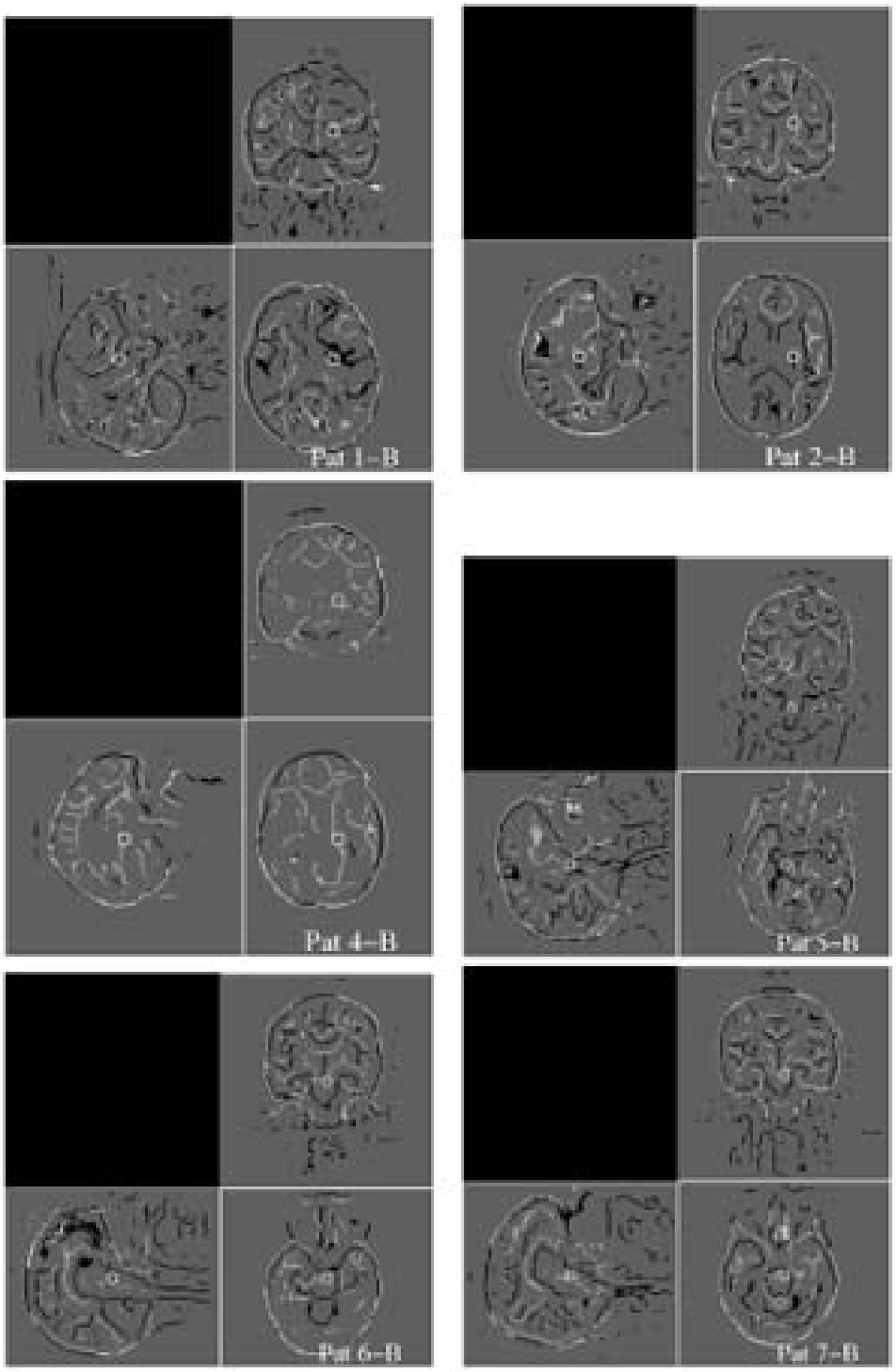

Figure B.4: Visual registration for patient 1–B, 2–B, 4–B, 5–B, 6–B and 7–B, modalities MR_RAGE to MR_T2